

Supplement of Atmos. Chem. Phys., 21, 989–1013, 2021  
<https://doi.org/10.5194/acp-21-989-2021-supplement>  
© Author(s) 2021. This work is distributed under  
the Creative Commons Attribution 4.0 License.



Atmospheric  
Chemistry  
and Physics  
Open Access  


*Supplement of*

## Aircraft-based observation of meteoric material in lower-stratospheric aerosol particles between 15 and 68° N

Johannes Schneider et al.

Correspondence to: Johannes Schneider (johannes.schneider@mpic.de)

The copyright of individual parts of the supplement might differ from the CC BY 4.0 License.

## **Introduction**

This document contains supplementary information, with the objective to give more background information on the data shown in the main article, to enable its interpretation to be scrutinised transparently. Firstly, the clustering methodology is explained in more detail, with the clustering parameters of the single particle data evaluation, and an associated uncertainty estimated (S1). Secondly (S2), the mean mass spectra and vertical profiles of the meteoric-particle abundance fractions for each of the five UTLS campaigns are shown in Figures S1 to S5. The data displayed in Figure 4 of the main text are shown for each of the individual missions in S3 (Figure S6). Section S4 (Figure S7) shows the O<sub>3</sub>-H<sub>2</sub>O tracer-tracer plot for StratoClim 2016 which was not used in the main text. The calculation of the sedimentation velocity is explained in S5. An example of sampling line loss calculation is presented in S6. Section S7 shows the results of Mie calculations used to convert the calibration data to real stratospheric refractive indices. More information on the detection of meteoric material in tropospheric particles at the Jungfraujoch is presented in S8. Finally, Section S9 explains how changing the threshold defining at what times stratospheric air was sampled affects the stratospheric proportions presented.

## **S1 Clustering Parameters**

### **Clustering algorithm and parameters**

The individual bipolar mass spectra were sorted using the fuzzy c-means algorithm (Bezdek et al., 1984; Hinz et al., 1999), using the software CRISP that was written at MPIC (Klimach et al., 2010; Klimach, 2012; Roth et al., 2016). The parameters are given in Table S1. Cations were used because the meteoric material is best recognized in the cation spectrum (Fe<sup>+</sup>, Mg<sup>+</sup>). Preprocessing is done by taking each ion signal to the power of 0.5 to reduce the influence of the signal intensity. The mass spectra were normalized to their sum to reduce the influence of the total ion count per spectrum. Linear correlation was used for the distance metric (defining "similarity" of the spectra), with a perfect Pearson correlation ( $r = 1$ ) meaning that two spectra are identical. The number of clusters was prescribed with 20. A set of starting cluster centers was chosen from the data set with the condition that these clusters have Pearson correlation coefficient smaller than 0.9. The fuzzifier (originally introduced as "weighting exponent" by Bezdek (1981) represents the fuzziness (blurring, defocusing) of the classification. "Fuzzy abort" parameter defines the convergence criterion of the algorithm, i.e. when the differences between subsequent cluster runs change by less than the chosen value, the algorithm ends.

### **Variation of clustering parameters**

To estimate the influence of the clustering parameters and the chosen sorting algorithm on the number of particles containing meteoric material, six additional different clustering runs were conducted for each UTLS mission. The varied parameters are: number of clusters (10, 20, 30), initialization cluster difference (0.9, 0.7), fuzzyfier (1.3, 1.5), preprocessing (power = 0.5, none), and algorithm type (fuzzy c-means, k-means). Table

S2 lists the different runs, the varied parameters and the resulting number of particles identified to contain meteoric material.

Criteria for selecting a certain cluster as "containing meteoric material" were 1) high cation signals of Fe<sup>+</sup> and Mg<sup>+</sup> (additionally allowing Na<sup>+</sup>, K<sup>+</sup>, Al<sup>+</sup>), 2) anion signal at HSO<sub>4</sub><sup>-</sup> or cation signals at S<sup>+</sup>, SO<sub>4</sub><sup>+</sup>, H<sub>3</sub>SO<sub>4</sub><sup>+</sup>, 3) vertical profile showing increasing fractional abundance with increasing altitude, potential temperature, or potential vorticity.

In general, the standard deviation is below 6% of the mean value, and the chosen final clustering result using the parameters given in Table S1 (printed in bold) is very close to the mean value.

## S2 Individual cluster properties.

Figures S1 through S5 show the particle clusters identified as "containing meteoric material" for each of the five UTLS aircraft missions. The cluster were selected following the criteria given in section S1.

## S3 Theta-latitude histograms for individual aircraft missions.

Figure S6 shows the theta-latitude histograms for each of the five UTLS aircraft missions, these data merged to produce Figure 4 of the main text.

## S4 Tracer-tracer correlation for StratoClim 2016.

The O<sub>3</sub> and H<sub>2</sub>O measurements during StratoClim 2016 did not cover the whole flight time of the three measurement flights. Thus, the data were not used in Figure 8 of the main text, but for completeness are shown here in Figure S7.

## S5 Particle sedimentation in the lower stratosphere.

The time scale for particle sedimentation was calculated as follows:

Pressure, temperature and viscosity of air were taken from the US Standard Atmosphere, using 100 m vertical resolution.

Mean free path ( $\lambda$ ), Knudsen number ( $Kn$ ), Cunningham correction ( $C_C$ ) and terminal settling velocity ( $V_{TS}$ ) were calculated using the following equations ((Hinds, 1999; Seinfeld and Pandis, 2006)):

$$\lambda = \frac{1}{\sqrt{2\pi d_m^2 N}} \quad (S1)$$

with  $d_m$  = collision diameter of air molecules ( $3.7 \times 10^{-10}$  m), and  $N$  = number density of air molecules,

$$Kn = \frac{2\lambda}{d} \quad (S2)$$

with  $d$  = particle diameter,

$$C_C = 1 + Kn \left( \alpha + \beta e^{-\frac{\gamma}{Kn}} \right), \quad (S3)$$

with  $\alpha = 1.155$ ,  $\beta = 0.471$ ,  $\gamma = 0.596$  (Allan and Raabe, 1982)

$$V_{TS} = \frac{\varrho d^2 g c_C}{18 \eta}, \quad (\text{S4})$$

with  $\varrho$  = particle density,  $g$  = acceleration of gravity,  $\eta$  = viscosity of air.

The terminal settling velocity was calculated for pure H<sub>2</sub>SO<sub>4</sub> particles ( $\varrho = 1.83 \text{ g cm}^{-3}$ ) and pure olivine particles ( $\varrho = 3.30 \text{ g cm}^{-3}$ ), assuming spherical particle shape. Figure S8 shows the terminal settling velocity as a function of altitude.

## S6 Sampling line transmission efficiency.

The sampling line transmission efficiency was calculated here as an example for the configuration of ML-CIRRUS (ALABAMA operated on the HALO aircraft). The  $\frac{1}{4}$ " stainless steel sampling line that connected the HALO aerosol submicrometer inlet (HASI, Wendisch et al. (2016); Andreae et al. (2018)) line had a total length of 2.9 m with several bends, horizontal and vertical sections. The calculations were done with a modified version of the Particle Loss Calculator (PLC) that was originally described in von der Weiden et al. (2009). The modified version allows for including the sampling line pressure. The results are shown in Figure S9.

## S7 Mie calculations for stratospheric aerosol for the optical particle spectrometers OPC 1.129 and UHSAS.

The response of the optical particle spectrometers OPC 1.129 and UHSAS for stratospheric aerosol particles was calculated using an in-house written software (Vetter, 2004) following the algorithms described in Bohren and Huffman (1983). The OPC 1.129 uses a laser wavelength of 655 nm. The scattered light is collected under  $90^\circ$  with an angular range of  $60^\circ$  (i.e.  $60^\circ - 120^\circ$ ). The UHSAS uses a laser wavelength of 1054 nm and collects the scattered light in an angular range between  $22^\circ$  and  $158^\circ$ . The refractive index for PSL,  $m = 1.59$ , was taken from Heim et al. (2008). The refractive index range ( $m = 1.43 - 1.45$ ) for lower stratospheric aerosol was taken from Yue et al. (1994).

The results (Figure S10) show that the lower size cut-off of the OPC shifts from 250 nm to about 285 nm when the refractive index for stratospheric aerosol is used. For the UHSAS, the lower cut-off of 180 nm (calibrated by PSL) increases to 200 nm.

## S8 Jungfraujoch backtrajectories, ozone mixing ratio, and meteoric particle fraction.

We inspected backtrajectories to obtain more information on the origin of the meteoric particles detected during the INUIT-2017 campaign at the Jungfraujoch station (3600 m altitude). For this, HYSPLIT (Stein et al., 2015) back trajectories were calculated for 120 – 143 hours using the GDAS 0.5 degree data set (NCEP meteorological re-analysis, Saha et al., 2010). We chose 3600 m a.s.l. as a starting point, with 27 trajectories started per hour, using the trajectory ensemble option. All trajectory data points were stratified into altitude and latitude bins and the number of trajectory points per grid is plotted in Figure S11 a) and b).

Panel c) of Figure S11 shows the time series of the fraction of meteoric particles detected along with the O<sub>3</sub> mixing ratio. The fraction of meteoric particles is found to be highest between the 18th and 21st of February, a period during which the air mass spent more time at higher altitudes and latitudes before arriving at the Jungfraujoch. A similar but less pronounced feature is found between 15th and 17th of February. These findings support the conclusion that the origin of this particle type is at higher altitudes. The dependence on latitude can be explained by the fact that mixing between stratosphere and troposphere is stronger at mid-latitudes (see Figure 8 in the main part) than in the tropics. Thus, we would expect to see a higher meteoric particle fraction when the air masses have experienced higher latitudes and altitudes, which is confirmed by Figure S11. Furthermore, a stratospheric origin is supported by the ozone trend in Panel c). The time trend of the meteoric particles follows closely the ozone time series, and even small-scale features (e.g. Feb. 09, Feb. 11, Feb. 16, and Feb. 22) are clearly visible in both time series.

## S9 Number of particles in the stratosphere

Table S3 shows the number of particle mass spectra measured in the stratosphere, for all particles and for meteoric particles. To test the sensitivity of the calculations, we used different definitions of the tropopause (PV > 2 PVU, PV > 4 PVU, O<sub>3</sub> > 150 ppbv, and pot. temp. > 380 K. The latter criterion could only be applied to the StratoClim data sets, because only the Geophysica reaches to 380 K. The ozone criterion could not be applied to the StratoClim 2016 data set due to low data coverage. As a final result, we decided to use PV > 4 PVU as the threshold for Table 1 in the main text.

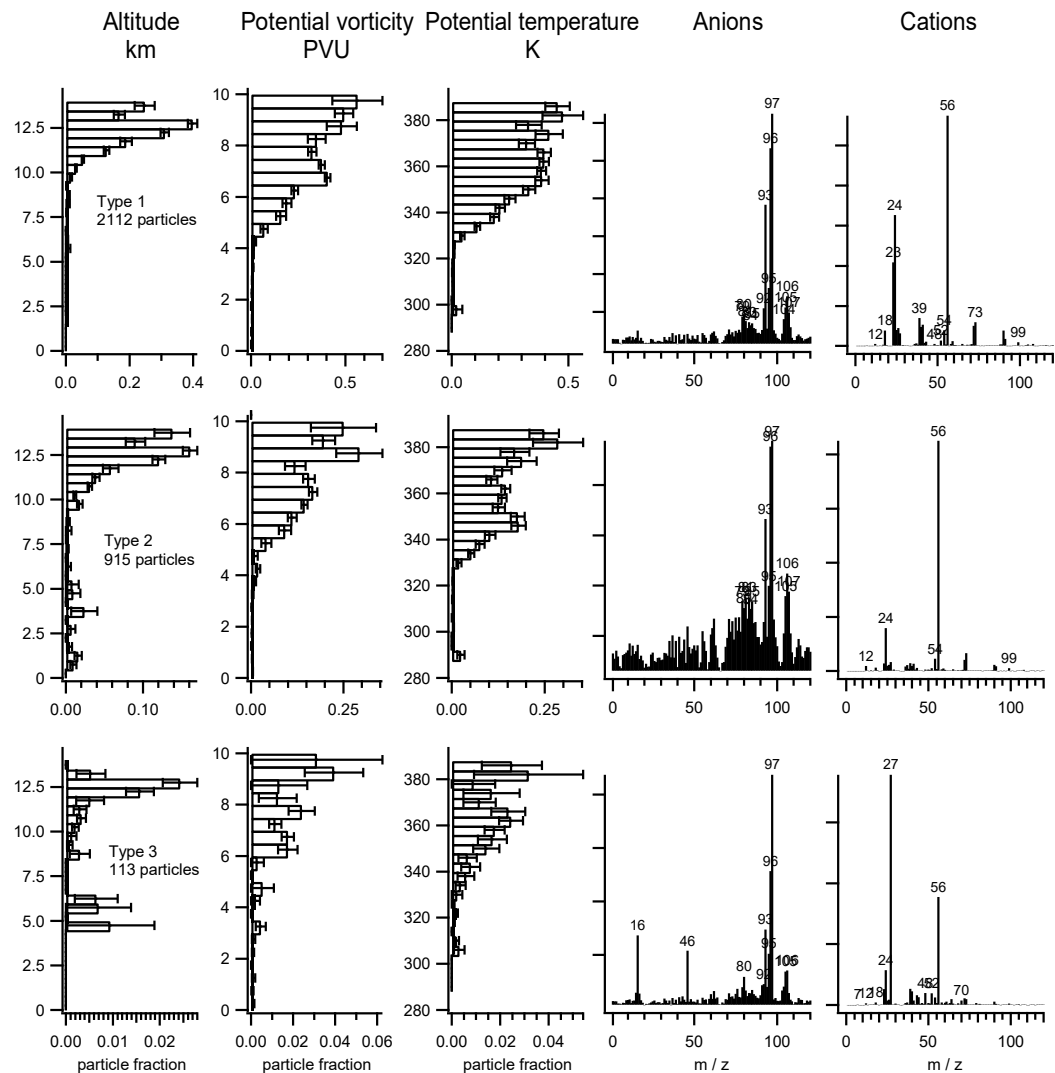


**Figure S1.** Vertical profiles and mean mass spectra of all clusters from the ML-CIRRUS 2014 data set interpreted as particles containing meteoric material. Note that the negative mass spectra (anions) are noisy, because all anion spectra of each cluster type were averaged for this display, also those where no anion signal was obtained.

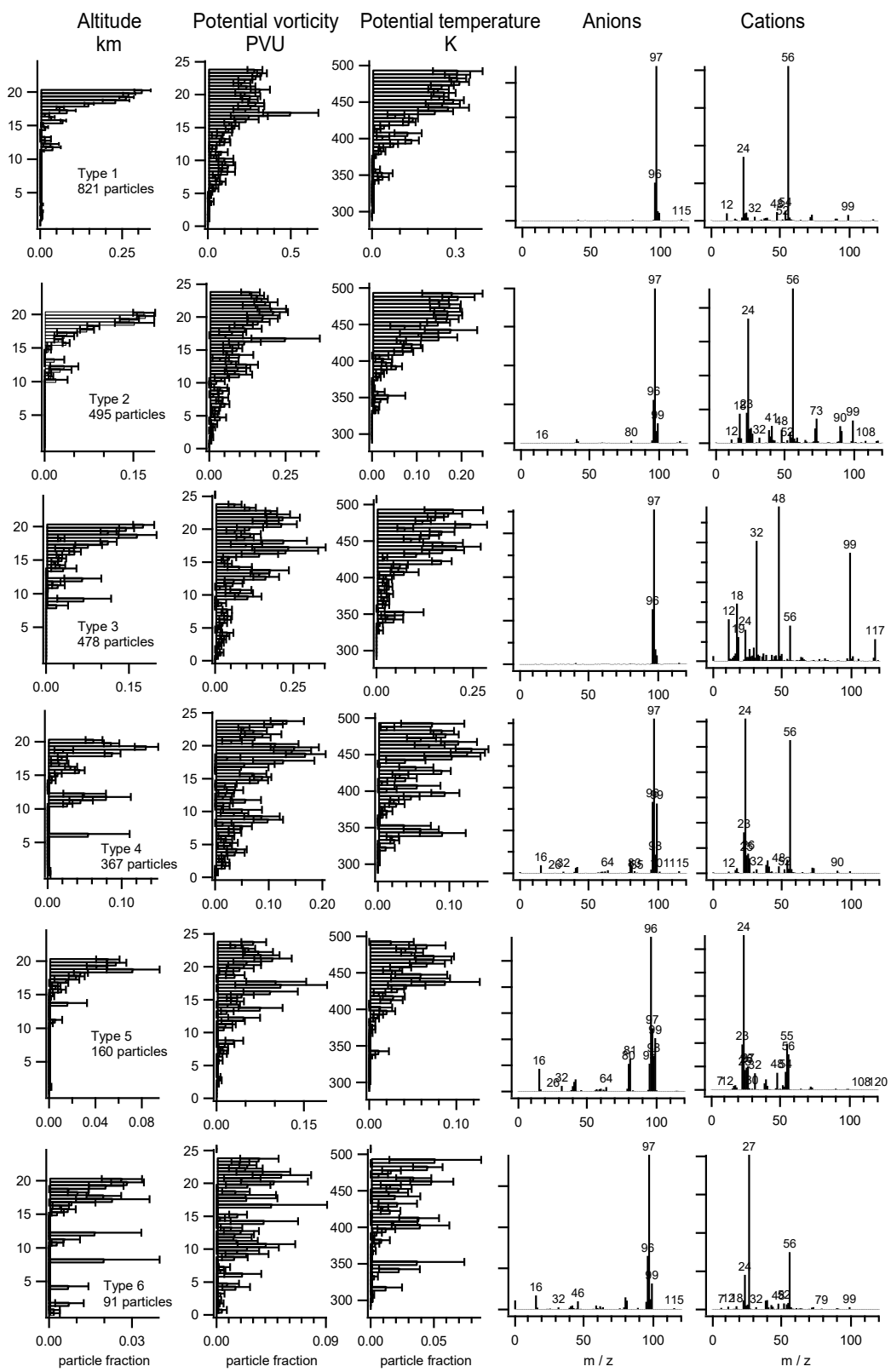


**Figure S2.** Vertical profiles and mean mass spectra of all clusters from the StratoClim 2016 data set interpreted as particles containing meteoric material.

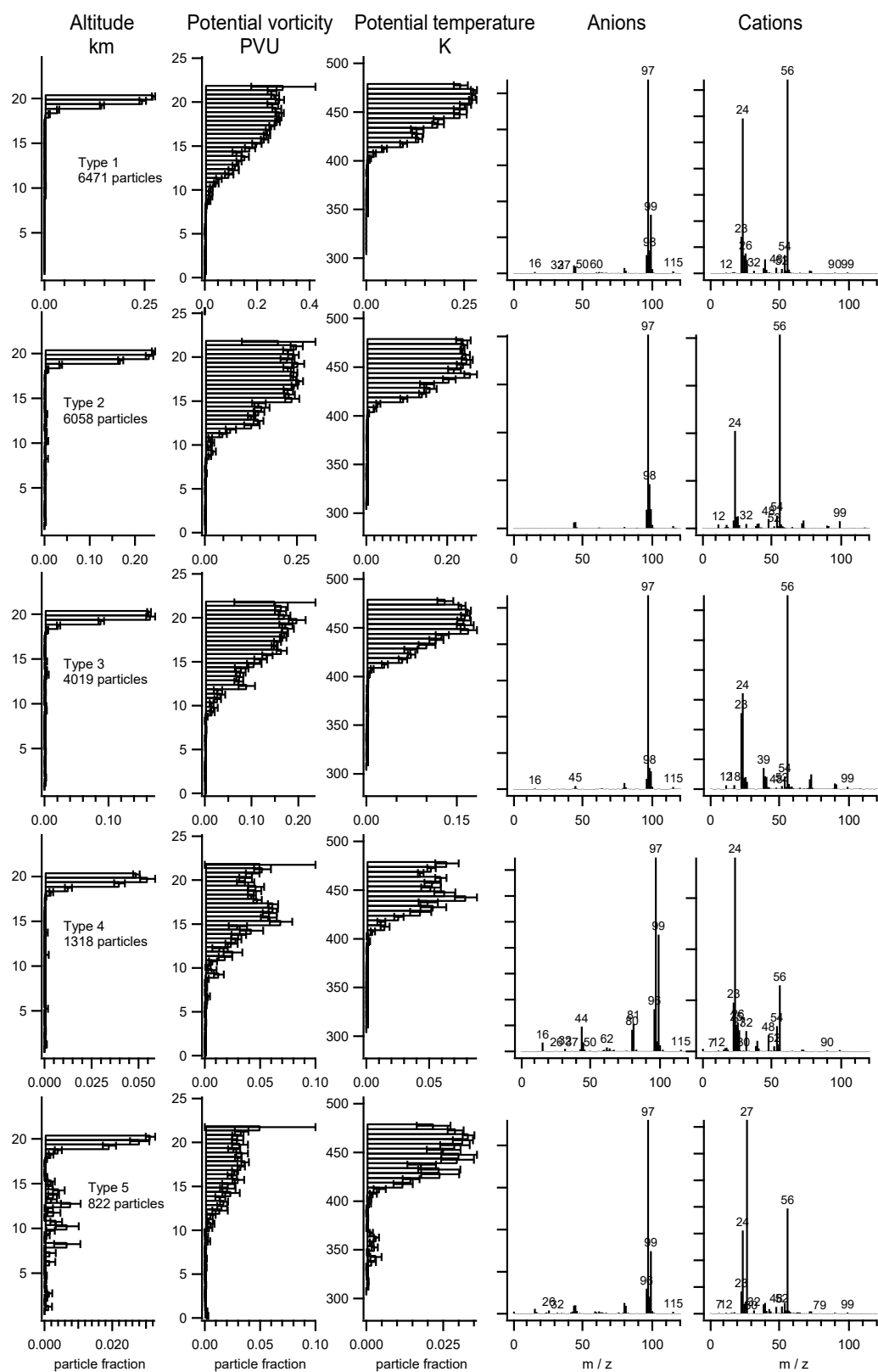


**Figure S3.** Vertical profiles and mean mass spectra of all clusters from the StratoClim 2017 data set interpreted as particles containing meteoric material.

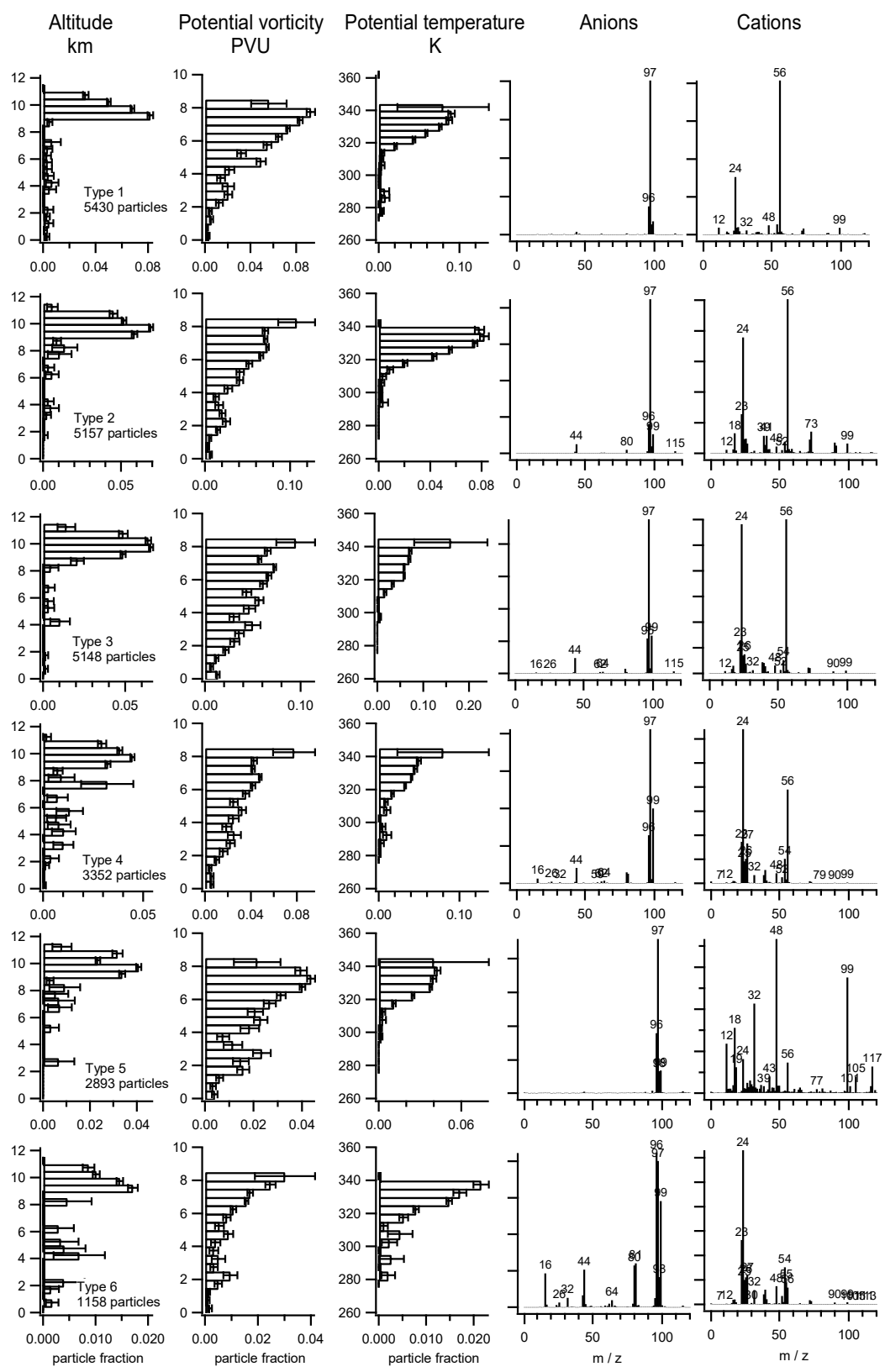


**Figure S4.** Vertical profiles and mean mass spectra of all clusters from the ND-MAX/ECLIF-2 data set interpreted as particles containing meteoric material.

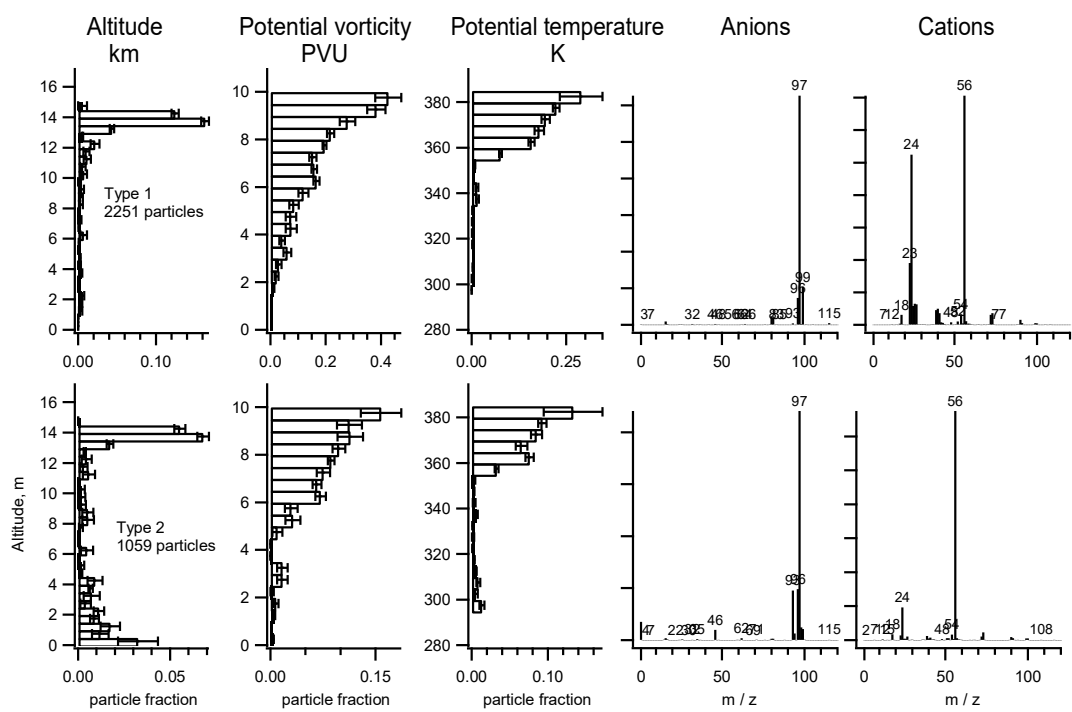


**Figure S5. Vertical profiles and mean mass spectra of all clusters from the CAFE-Africa data set interpreted as particles containing meteoric material.**

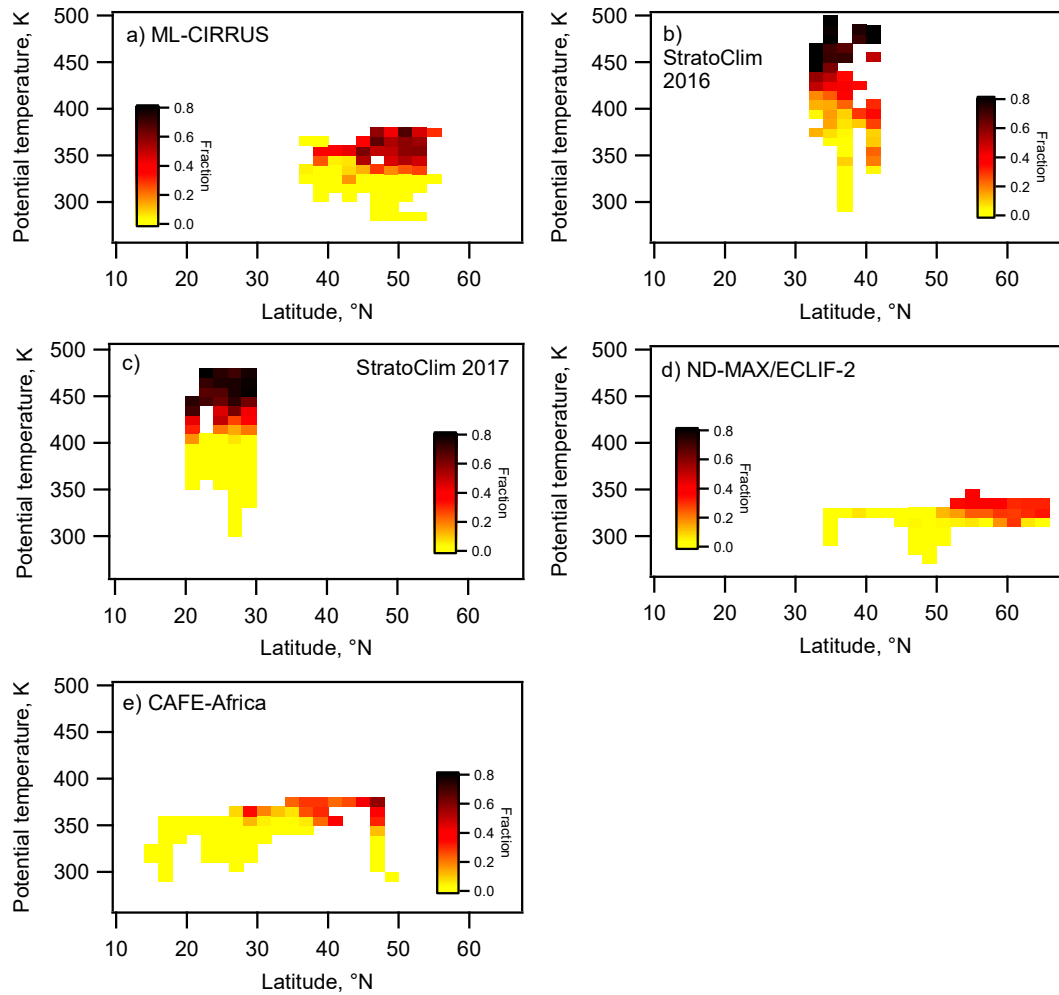


**Figure S6. Fraction of meteoric particles as function of potential temperature and latitude for the individual missions: a) ML-CIRRUS, b) StratoClim 2016, c) StratoClim 2017, d) ND-MAX-ECLIF-2, e) CAFE-Africa.**

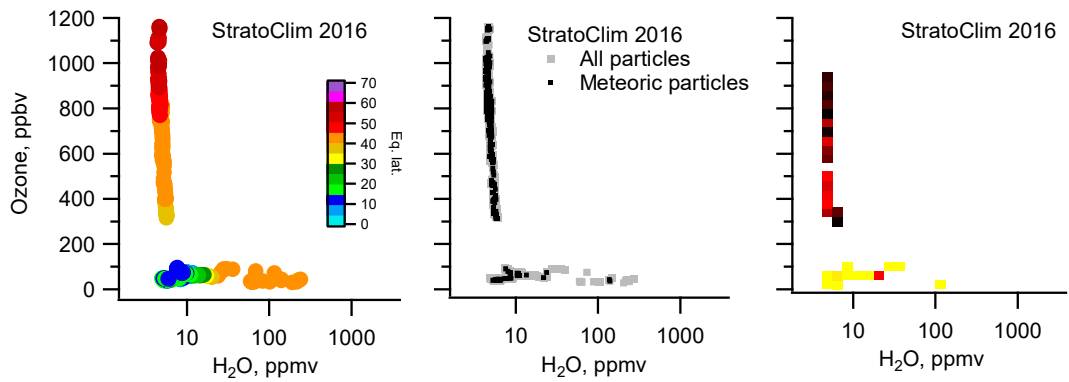


**Figure S7. Tracer-tracer correlation for StratoClim 2016.** As the instruments were not fully operative during the whole flight time of the three flights of StratoClim 2016, several gaps in the data prevent the analysis of cross-tropopause transport for this mission.

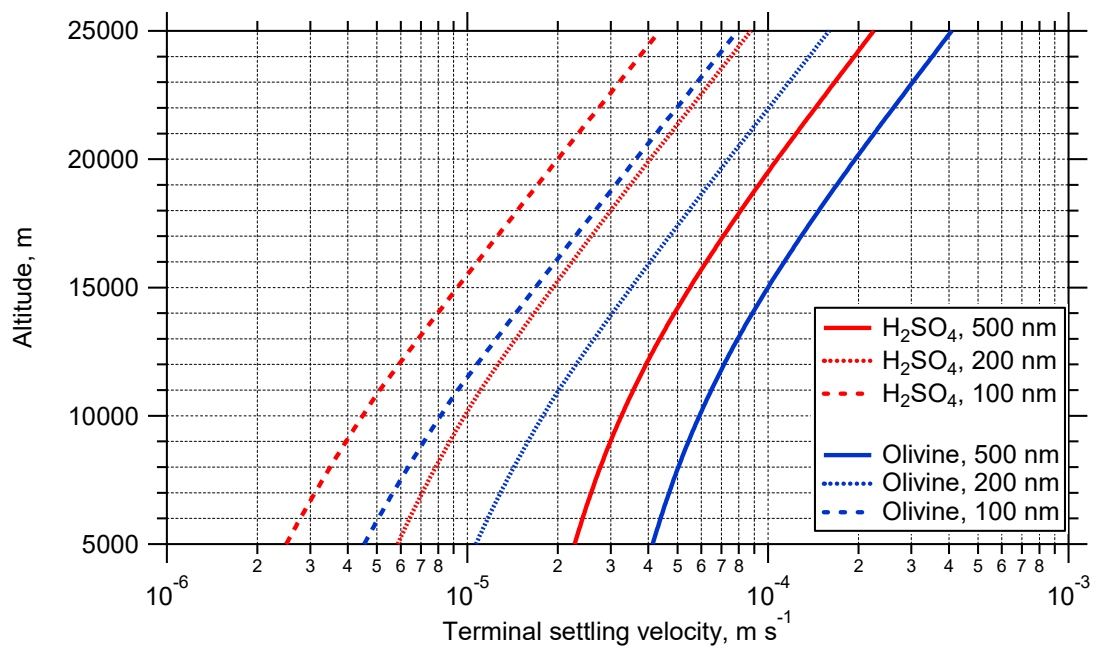


**Figure S8.** Terminal settling velocity for H<sub>2</sub>SO<sub>4</sub> and olivine particles of 100, 200, and 500 nm volume equivalent diameter ( $d_{ve}$ ).

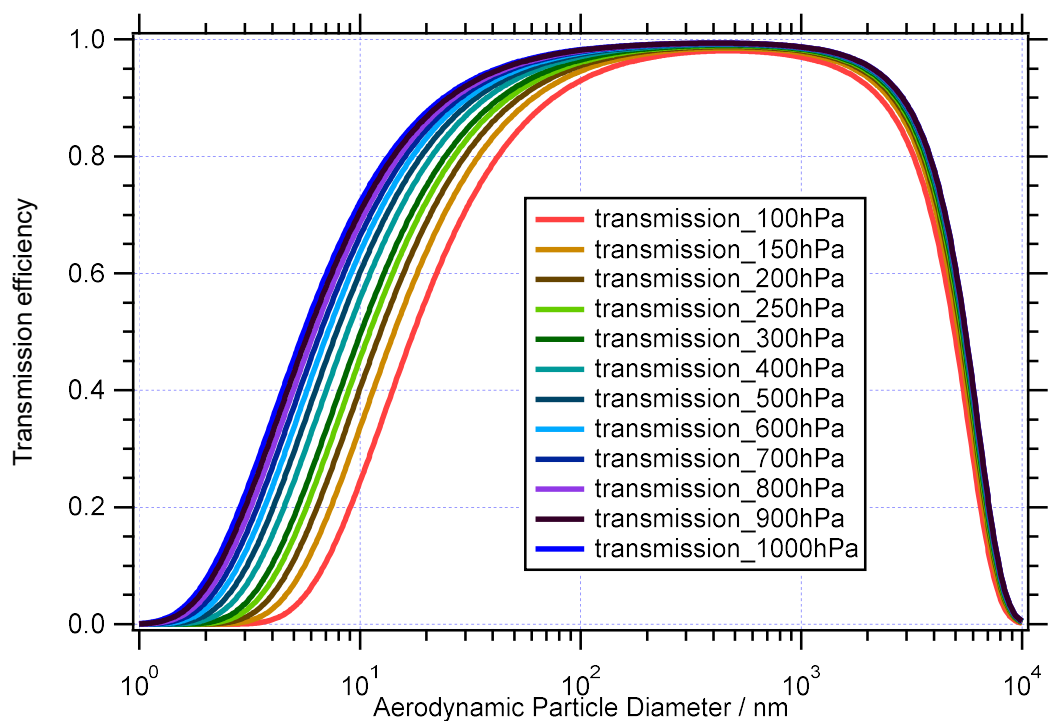


**Figure S9. Transmission curves for the sampling line used in ML-CIRRUS that connected the HALO aerosol submicrometer inlet (HASI) to the OPC 1.129 in the ALABAMA rack.**

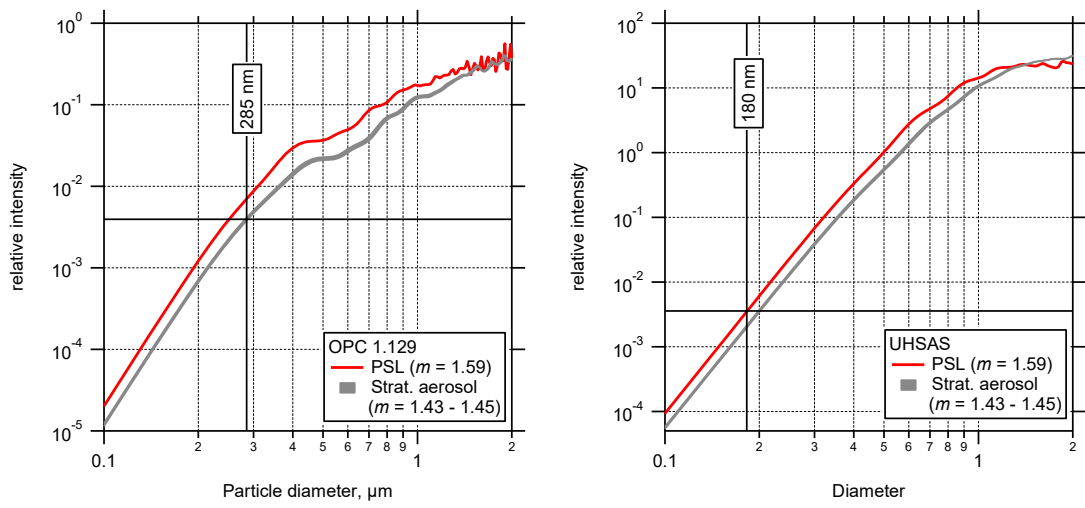


**Figure S10.** Relative intensity at the detector calculated for the OPC (Grimm 1.129, "Sky-OPC") and for the UHSAS, for PSL particles and for stratospheric particles.

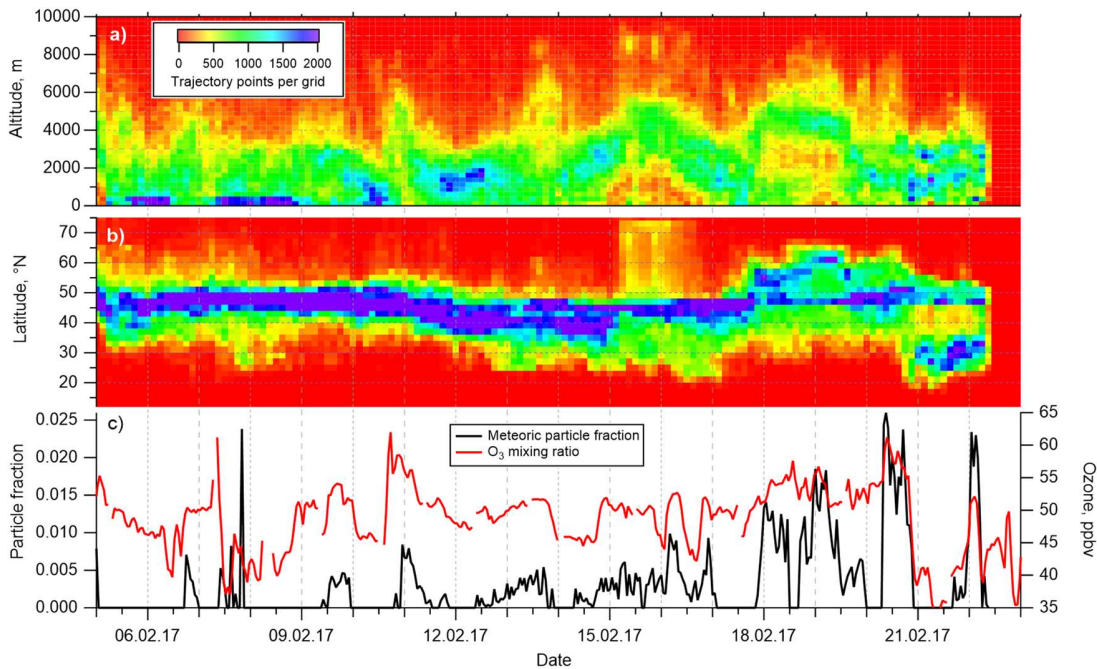


**Figure S11.** Backtrajectory information for the INUIT-JFJ 2017 field campaign at Jungfraujoch. For each hour, 27 backtrajectories were started using the trajectory ensemble option and were followed for 120 – 143 h using HYSPLIT [Stein et al., 2015] with the GADS 0.5 degree data set. Panel a) shows the number of points during which the trajectories resided in the respective altitude and time grid, Panel b) the same but for latitude. Panel c) shows the number fraction of the meteoric particles along with ozone mixing ratio.

|                    |                          |
|--------------------|--------------------------|
| Ion type           | Cations                  |
| Preprocessing      | Power each m/z by 0.5    |
| Normalization      | Sum                      |
| Distance metric    | Correlation              |
| Initialization     | Different startclusters: |
| Number of clusters | 20                       |
| Cluster difference | 0.9                      |
| Fuzzifier          | 1.3                      |
| Fuzzy abort        | 1e-5                     |

Table S1. Clustering parameters used for the final analysis.

| Project            | Cluster algorithm    | Number of clusters | Cluster diff | Fuzzifier  | Pre-processing                  | Number of "meteoric" particles |
|--------------------|----------------------|--------------------|--------------|------------|---------------------------------|--------------------------------|
| ML-CIRRUS          | Fuzzy c-means        | 10                 | 0.9          | 1.3        | $(m/z)^{0.5}$                   | 3080                           |
|                    | <b>Fuzzy c-means</b> | <b>20</b>          | <b>0.9</b>   | <b>1.3</b> | <b><math>(m/z)^{0.5}</math></b> | <b>3140</b>                    |
|                    | Fuzzy c-means        | 30                 | 0.9          | 1.3        | $(m/z)^{0.5}$                   | 3136                           |
|                    | Fuzzy c-means        | 20                 | 0.7          | 1.3        | $(m/z)^{0.5}$                   | 2931                           |
|                    | Fuzzy c-mean         | 20                 | 0.9          | 1.5        | $(m/z)^{0.5}$                   | 3136                           |
|                    | Fuzzy c-means        | 20                 | 0.9          | 1.3        | none                            | 3051                           |
|                    | k-means              | 20                 | 0.9          | N/A        | $(m/z)^{0.5}$                   | 3247                           |
| Mean ± StdDev      |                      |                    |              |            |                                 | 3103 ± 90                      |
| StratoClim<br>2016 | Fuzzy c-means        | 10                 | 0.9          | 1.3        | $(m/z)^{0.5}$                   | 2357                           |
|                    | <b>Fuzzy c-means</b> | <b>20</b>          | <b>0.9</b>   | <b>1.3</b> | <b><math>(m/z)^{0.5}</math></b> | <b>2412</b>                    |
|                    | Fuzzy c-means        | 30                 | 0.9          | 1.3        | $(m/z)^{0.5}$                   | 2679                           |
|                    | Fuzzy c-means        | 20                 | 0.7          | 1.3        | $(m/z)^{0.5}$                   | 2376                           |
|                    | Fuzzy c-mean         | 20                 | 0.9          | 1.5        | $(m/z)^{0.5}$                   | 2567                           |
|                    | Fuzzy c-means        | 20                 | 0.9          | 1.3        | none                            | 2618                           |
|                    | k-means              | 20                 | 0.9          | N/A        | $(m/z)^{0.5}$                   | 2570                           |
| Mean ± StdDev      |                      |                    |              |            |                                 | 2511 ± 118                     |
| StratoClim<br>2017 | Fuzzy c-means        | 10                 | 0.9          | 1.3        | $(m/z)^{0.5}$                   | 18355                          |
|                    | <b>Fuzzy c-means</b> | <b>20</b>          | <b>0.9</b>   | <b>1.3</b> | <b><math>(m/z)^{0.5}</math></b> | <b>18688</b>                   |
|                    | Fuzzy c-means        | 30                 | 0.9          | 1.3        | $(m/z)^{0.5}$                   | 19700                          |
|                    | Fuzzy c-means        | 20                 | 0.7          | 1.3        | $(m/z)^{0.5}$                   | 18688                          |
|                    | Fuzzy c-mean         | 20                 | 0.9          | 1.5        | $(m/z)^{0.5}$                   | 18459                          |
|                    | Fuzzy c-means        | 20                 | 0.9          | 1.3        | none                            | 21235                          |
|                    | k-means              | 20                 | 0.9          | N/A        | $(m/z)^{0.5}$                   | 20215                          |
| Mean ± StdDev      |                      |                    |              |            |                                 | 19334 ± 1006                   |
| ND-MAX/<br>ECLIF-2 | Fuzzy c-means        | 10                 | 0.9          | 1.3        | $(m/z)^{0.5}$                   | 20141                          |
|                    | <b>Fuzzy c-means</b> | <b>20</b>          | <b>0.9</b>   | <b>1.3</b> | <b><math>(m/z)^{0.5}</math></b> | <b>23138</b>                   |
|                    | Fuzzy c-means        | 30                 | 0.9          | 1.3        | $(m/z)^{0.5}$                   | 21883                          |
|                    | Fuzzy c-means        | 20                 | 0.7          | 1.3        | $(m/z)^{0.5}$                   | 21681                          |
|                    | Fuzzy c-mean         | 20                 | 0.9          | 1.5        | $(m/z)^{0.5}$                   | 21126                          |
|                    | Fuzzy c-means        | 20                 | 0.9          | 1.3        | none                            | 21752                          |
|                    | k-means              | 20                 | 0.9          | N/A        | $(m/z)^{0.5}$                   | 18998                          |
| Mean ± StdDev      |                      |                    |              |            |                                 | 21245 ± 1237                   |
| CAFE-Africa        | Fuzzy c-means        | 10                 | 0.9          | 1.3        | $(m/z)^{0.5}$                   | 3325                           |
|                    | <b>Fuzzy c-means</b> | <b>20</b>          | <b>0.9</b>   | <b>1.3</b> | <b><math>(m/z)^{0.5}</math></b> | <b>3310</b>                    |
|                    | Fuzzy c-means        | 30                 | 0.9          | 1.3        | $(m/z)^{0.5}$                   | 3290                           |
|                    | Fuzzy c-means        | 20                 | 0.7          | 1.3        | $(m/z)^{0.5}$                   | 3194                           |
|                    | Fuzzy c-mean         | 20                 | 0.9          | 1.5        | $(m/z)^{0.5}$                   | 3281                           |
|                    | Fuzzy c-means        | 20                 | 0.9          | 1.3        | none                            | 3287                           |
|                    | k-means              | 20                 | 0.9          | N/A        | $(m/z)^{0.5}$                   | 3515                           |
| Mean ± StdDev      |                      |                    |              |            |                                 | 3314 ± 90                      |

Table S2. Variations of clustering parameters. The inferred number of particles containing meteoric material is given in the last column. Other parameters were kept as in Table S1.

a) All particles

|           | PV > 2 | PV > 4 | O3 > 150 | Theta > 380 |
|-----------|--------|--------|----------|-------------|
| ML-CIRRUS | 13029  | 6509   | 6174     | N/A         |
| SC16      | 6662   | 5092   | N/A      | 4874        |
| SC17      | 76856  | 51599  | 41146    | 57109       |
| NDMAX     | 78454  | 73367  | 72923    | N/A         |
| CAFE      | 12161  | 10771  | 9441     | N/A         |

b) Meteoric particles

|           | PV > 2 | PV > 4 | O3 > 150 | Theta > 380 |
|-----------|--------|--------|----------|-------------|
| ML-CIRRUS | 3063   | 2986   | 2477     | N/A         |
| SC16      | 2363   | 2271   | N/A      | 2238        |
| SC17      | 18487  | 18421  | 18016    | 18450       |
| NDMAX     | 22626  | 22050  | 22104    | N/A         |
| CAFE      | 2946   | 2882   | 2789     | N/A         |

c) Proportion

|           | PV > 2 | PV > 4 | O3 > 150 | Theta > 380 |
|-----------|--------|--------|----------|-------------|
| ML-CIRRUS | 0.235  | 0.459  | 0.401    | N/A         |
| SC16      | 0.355  | 0.446  | N/A      | 0.459       |
| SC17      | 0.241  | 0.357  | 0.438    | 0.323       |
| NDMAX     | 0.228  | 0.301  | 0.303    | N/A         |
| CAFE      | 0.242  | 0.268  | 0.295    | N/A         |

Table S3. a) Number of analyzed particles in the stratosphere; b) number of meteoric particles in the stratosphere, c) proportion (numbers in b) divided by numbers in a)). Different criteria were used to define the tropopause. For Table 1 and Figure 6 in the main text, PV > 4 was selected for the following reasons: to avoid the mixing regime at mid-latitudes and to match the tropical 380 K tropopause definition (see also (Ploeger et al., 2015)).

## References

- Andreae, M. O., Afchine, A., Albrecht, R., Holanda, B. A., Artaxo, P., Barbosa, H. M. J., Borrmann, S., Cecchini, M. A., Costa, A., Dollner, M., Fütterer, D., Järvinen, E., Jurkat, T., Klimach, T., Konemann, T., Knote, C., Krämer, M., Krisna, T., Machado, L. A. T., Mertes, S., Minikin, A., Pöhlker, C., Pöhlker, M. L., Pöschl, U., Rosenfeld, D., Sauer, D., Schlager, H., Schnaiter, M., Schneider, J., Schulz, C., Spanu, A., Sperling, V. B., Voigt, C., Walser, A., Wang, J., Weinzierl, B., Wendisch, M., and Ziereis, H.: Aerosol characteristics and particle production in the upper troposphere over the Amazon Basin, *Atmos. Chem. Phys.*, 18, 921-961, 10.5194/acp-18-921-2018, 2018.
- Bezdek, J. C.: *Pattern Recognition with Fuzzy Objective Function Algorithms*, Plenum Press, New York, USA, 1981.
- Bezdek, J. C., Ehrlich, R., and Full, W.: FCM: The fuzzy c-means clustering algorithm, *Computers & Geosciences*, 10, 191-203, 10.1016/0098-3004(84)90020-7, 1984.
- Bohren, C. F., and Huffman, D. R.: *Absorption and scattering of light by small particles*, Wiley and Sons, New York, 1983.
- Heim, M., Mullins, B. J., Umhauer, H., and Kasper, G.: Performance evaluation of three optical particle counters with an efficient “multimodal” calibration method, *J. Aerosol. Sci.*, 39, 1019-1031, <https://doi.org/10.1016/j.jaerosci.2008.07.006>, 2008.
- Hinds, W. C.: *Aerosol technology - properties, behaviour, and measurements of airborne particles*, 2. ed., John Wiley & Sons, Inc., New York, 1999.
- Hinz, K. P., Greweling, M., Drews, F., and Spengler, B.: Data processing in on-line laser mass spectrometry of inorganic, organic, or biological airborne particles, *Journal of the American Society for Mass Spectrometry*, 10, 648-660, 10.1016/s1044-0305(99)00028-8, 1999.
- Klimach, T., Drewnick, F., and Borrmann, S.: CRISP - a new tool for analysis of single particle mass spectra, International Aerosol Conference, Helsinki, 2010.
- Klimach, T.: Chemische Zusammensetzung der Aerosole: Design und Datenauswertung eines Einzelpartikel-Laserablationsmassenspektrometers, Johannes Gutenberg-Universität, Mainz, Germany, 2012.
- Ploeger, F., Gottschling, C., Griessbach, S., Groß, J. U., Guenther, G., Konopka, P., Müller, R., Riese, M., Stroh, F., Tao, M., UngermaNN, J., Vogel, B., and von Hobe, M.: A potential vorticity-based determination of the transport barrier in the Asian summer monsoon anticyclone, *Atmos. Chem. Phys.*, 15, 13145-13159, 10.5194/acp-15-13145-2015, 2015.
- Roth, A., Schneider, J., Klimach, T., Mertes, S., van Pinxteren, D., Herrmann, H., and Borrmann, S.: Aerosol properties, source identification, and cloud processing in orographic clouds measured by single particle mass spectrometry on a central European mountain site during HCCT-2010, *Atmos. Chem. Phys.*, 16, 505-524, 10.5194/acp-16-505-2016, 2016.
- Saha, S., Moorthi, S., Pan, H. L., Wu, X. R., Wang, J. D., Nadiga, S., Tripp, P., Kistler, R., Woollen, J., Behringer, D., Liu, H. X., Stokes, D., Grumbine, R., Gayno, G., Wang, J., Hou, Y. T., Chuang, H. Y., Juang, H. M. H., Sela, J., Iredell, M., Treadon, R., Kleist, D., Van Delst, P., Keyser, D., Derber, J., Ek, M., Meng, J., Wei, H. L., Yang, R. Q., Lord, S., Van den Dool, H., Kumar, A., Wang, W. Q., Long, C., Chelliah, M., Xue, Y., Huang, B. Y., Schemm, J. K., Ebisuzaki, W., Lin, R., Xie, P. P., Chen, M. Y., Zhou, S. T., Higgins, W., Zou, C. Z., Liu, Q. H., Chen, Y., Han, Y., Cucurull, L., Reynolds, R. W., Rutledge, G., and Goldberg, M.: THE NCEP CLIMATE FORECAST SYSTEM REANALYSIS, *Bulletin of the American Meteorological Society*, 91, 1015-1057, 10.1175/2010bams3001.1, 2010.
- Seinfeld, J. H., and Pandis, S. N.: *Atmospheric chemistry and physics: from air pollution to climate change* John Wiley and Sons, Hoboken, NJ, 2006.

- Stein, A. F., Draxler, R. R., Rolph, G. D., Stunder, B. J. B., Cohen, M. D., and Ngan, F.: NOAA's HYSPLIT Atmospheric Transport and Dispersion Modeling System, Bulletin of the American Meteorological Society, 96, 2059-2077, doi:10.1175/BAMS-D-14-00110.1, 2015.
- Vetter, T.: Berechnung der Mie-Streufunktionen zur Kalibrierung optischer Partikelzähler, Diploma thesis (in German), University Mainz, 2004.
- von der Weiden, S. L., Drewnick, F., and Borrmann, S.: Particle Loss Calculator – a new software tool for the assessment of the performance of aerosol inlet systems, *Atmos. Meas. Tech.*, 2, 479-494, 10.5194/amt-2-479-2009, 2009.
- Wendisch, M., Pöschl, U., Andreae, M. O., Machado, L. A. T., Albrecht, R., Schlager, H., Rosenfeld, D., Martin, S. T., Abdelmonem, A., Afchine, A., Araújo, A. C., Artaxo, P., Aufmhoff, H., Barbosa, H. M. J., Borrmann, S., Braga, R., Buchholz, B., Cecchini, M. A., Costa, A., Curtius, J., Dollner, M., Dorf, M., Dreiling, V., Ebert, V., Ehrlich, A., Ewald, F., Fisch, G., Fix, A., Frank, F., Fütterer, D., Heckl, C., Heidelberg, F., Hüneke, T., Jäkel, E., Järvinen, E., Jurkat, T., Kanter, S., Kästner, U., Kenntner, M., Kesselmeier, J., Klimach, T., Knecht, M., Kohl, R., Kölling, T., Krämer, M., Krüger, M., Krisna, T. C., Lavric, J. V., Longo, K., Mahnke, C., Manzi, A. O., Mayer, B., Mertes, S., Minikin, A., Molleker, S., Münch, S., Nillius, B., Pfeilsticker, K., Pöhlker, C., Roiger, A., Rose, D., Rosenow, D., Sauer, D., Schnaiter, M., Schneider, J., Schulz, C., de Souza, R. A. F., Spanu, A., Stock, P., Vila, D., Voigt, C., Walser, A., Walter, D., Weigel, R., Weinzierl, B., Werner, F., Yamasoe, M. A., Ziereis, H., Zinner, T., and Zöger, M.: ACRIDICON–CHUVA Campaign: Studying Tropical Deep Convective Clouds and Precipitation over Amazonia Using the New German Research Aircraft HALO, Bulletin of the American Meteorological Society, 97, 1885-1908, 10.1175/BAMS-D-14-00255.1, 2016.
- Yue, G. K., Poole, L. R., Wang, P. H., and Chiou, E. W.: Stratospheric aerosol acidity, density, and refractive-index deduced from SAGE-II and NMC temperature data, *J. Geophys. Res.-Atmos.*, 99, 3727-3738, 10.1029/93jd02989, 1994.